



Amplification of PEC hydrogen production through synergistic modification of Cu₂O using cadmium as buffer layer and dopant

Sanjib Shyamal^a, Arjun Maity^{b,c}, Ashis Kumar Satpati^d, Chinmoy Bhattacharya^{a,*}



^a Department of Chemistry, Indian Institute of Engineering Science & Technology, (IIEST), Shibpur, Howrah 711103, West Bengal, India

^b DST/CSIR Innovation Centre, National Centre for Nanostructured Materials, Pretoria 0001, South Africa

^c University of Johannesburg, Department of Applied Chemistry, South Africa

^d Analytical Chemistry Division, Bhabha Atomic Research Centre, Trombay, Mumbai 400085, India

ARTICLE INFO

Keywords:

One pot electro-synthesis
Cd modified Cu₂O semiconductor
Photoelectrochemical hydrogen production
Carrier concentration
Transit time

ABSTRACT

A facile single step electro-synthesis is applied to develop Cu/Cu₂O/Cd(OH)₂ thin films from the alkaline copper sulfate solution in presence of different levels of Cd²⁺. Cadmium implemented a synergistic effect, in the modification of Cu₂O, through the diffusion into the bulk Cu₂O and formation of Cd(OH)₂ buffer layer. The photoelectrochemical (PEC) performances of the optimized Cu/Cu₂O/Cd(OH)₂, significantly enhance the H⁺ reduction photocurrent to ~6.1 mA/cm² (1.5 times than that of pure Cu/Cu₂O) and the solar energy conversion efficiency also improve up to 5.8%, which is 2 fold higher than the pure semiconductor. Experimental evidences, including SEM-EDX, XRD, Raman, XPS and EIS confirm that Cd modifies Cu₂O through lowering the particle size with better crystallinity (accractive working surface area), minimizing resistance, increasing carrier concentration and rapid transfer of photogenerated charge carrier, resulting in suppression in electron-hole recombination, which facilitates the improved PEC performances.

1. Introduction

Cuprous oxide (Cu₂O), a p-type semiconductor, with direct band gap energy of 2.1 eV, chosen as the most promising photocatalyst for hydrogen production through water splitting in presence of sunlight [1–3]. Due to its natural abundance, high-absorption coefficient, low cost and non toxic nature, it attracts much interest for opto-electronic applications. The theoretical limit of the measured photocurrent for water splitting reaction using Cu₂O photocathode is as high as -14.7 mA/cm² under 1 sun illumination (AM 1.5 G) [4]. In order to achieve this photocurrent over Cu₂O, some modifications are essential. Low electrical mobility of the photogenerated charge carriers is one of the primary drawbacks for Cu₂O to act as an efficient photocatalyst for water splitting process. To overcome the hurdle, strategies for lowering of internal resistance (electrical) and increasing separation of photo-generated charge carriers are the key factors for photoelectrochemical (PEC) applications. There are many reports towards enhancement of efficiency of photo-assisted splitting of water, including homo or hetero-junction systems [5,6], doping [7,8], swift heavy-ion irradiation, applications of electro-catalysts etc [9–17]. In a recent study, we have demonstrated that PEC water splitting efficiency improves when better ohmic contact imported between Cu₂O and substrate [18,19]. It has

been reported that the lowest resistivity of 9 Ω-cm was obtained when cadmium (Cd), as a p-type dopant is incorporated to the bulk Cu₂O [20]. In one of the studies, resistance of the Cu₂O photocathode decreases by chlorine doping due to an increase of hole concentration while maintaining Hall mobility [21]. This particular change was justified by formation of an acceptor which could originate from either chlorine injection at an interstitial site in the lattice or a copper vacancy produced due to charge compensation effects that result when chlorine substitutes for an oxygen site and acts as a donor. Again introduction of suitable buffer layer (Ga₂O₃ and ZnO) [22,23] over the Cu₂O photocathode through the formation of n-p heterojunction are expected to increase the water splitting photocurrent by forming a favorable energy band alignment across the layer restricting the interfacial recombination. In comparison, the reported “modifications of Cu₂O thin film using buffer layer” employed step wise growth of the semiconductor matrix flowed by Atomic layer deposition of the ‘buffer layers’ which require highly sophisticated experimental set up and special condition for the film growth.

Herein, for the first time we demonstrate the combined effects of Cd diffusion into Cu/Cu₂O thin films and formation of Cd(OH)₂ buffer layer to enhance the water splitting photocurrent. A successful one pot synthetic route has been developed to fabricate Cu/Cu₂O/Cd(OH)₂

* Corresponding author.

E-mail addresses: cbhattacharya.besus@gmail.com, chinmoy@chem.iests.ac.in (C. Bhattacharya).

system in presence of different level of Cd^{2+} to the alkaline Cu^{2+} electrolytic bath. At an optimized condition, the $\text{Cu}/\text{Cu}_2\text{O}$ with 33% Cd, provides the highest photocurrent up to -6.1 mA/cm^2 for water reduction reaction at low onset potential. As far as literature reports are concerned, this is the highest reported photocurrent using p – Cu_2O without employing hydrogen evolution catalyst (Table S3, Supplementary material). The detailed PEC and physicochemical characterizations confirms, Cu_2O photocathode successfully modified with $\text{Cd}(\text{OH})_2$ buffer layer and Cd diffused in the bulk Cu_2O with lowering resistance, increasing hole concentration and discontinuing the conduction band, favorable for efficient water splitting reaction.

2. Experimental section

2.1. Materials

Copper sulfate (CuSO_4 , 5 H_2O), cadmium chloride (CdCl_2 , H_2O), dipotassium hydrogen phosphate (K_2HPO_4), lactic acid ($\text{CH}_3\text{CH}(\text{OH})\text{COOH}$), sodium-acetate (CH_3COONa), acetic acid (CH_3COOH), Triton X-100 surfactant (TX-100), potassium hydroxide (KOH), and sodium sulfate (Na_2SO_4 , 10 H_2O) were purchased from Merck (AR grade). High purity (> 99.9%) Cu foil was used as substrates to develop thin film Cu_2O semiconductors following proper cleaning with ethanol and Milli-Q water.

2.2. Fabrication of photoelectrodes

Cu_2O thin film semiconductors were electrodeposited from the aqueous electrolytic bath containing 0.2(M) Cu^{2+} and 3(M) lactic acid (used as a complexing agent) in the presence of 0.5(M) K_2HPO_4 buffer, 1% TX-100 and different levels of Cd^{2+} (10, 20, 25, 30, 33, 35, 45%) in the form of cadmium chloride. The pH ~ 12 of the electrolytic bath was maintained with addition of 2(M) KOH solution. At first Cd^{2+} solutions were prepared with subsequent addition of K_2HPO_4 , CuSO_4 , lactic acid, KOH and TX-100 surfactant. The thin films were developed on Cu substrate with an exposed area of $(1 \times 1) \text{ cm}^2$ (keeping other side insulated) under galvanostatic mode (-0.1 mA/cm^2 constant current density was applied) using a Metravi source meter in a standard two-electrode cell (a Pt foil counter electrode) at 30 °C for 3 h.

3. Film characterization

3.1. Physicochemical characterization

The surface morphology of the prepared samples were analyzed through field emission scanning electron microscope (Carl Zeiss Auriga, FEG SEM) using secondary electron operated at 5 kV accelerating voltage and the Smart SEM software. Elemental mapping was performed using an Oxford EDX detector and Aztec software. The crystalline nature of the prepared films were obtained through X-ray diffraction (XRD) analysis using Bruker AXS D8 Discover Diffractometer operated with Cu K_α radiation ($\lambda = 1.54 \text{ \AA}$), within the 2θ range of 20 - 80° at a scan speed of 2°/min. The Raman spectra were obtained using a Horiba Jobin-Yvon HR800 Raman spectrometer equipped with an Olympus BX-41 optical microscope. An Argon laser (514.5 nm) with a power setting of ~ 1.2 mW (Coherent Innova Model 308) was used as an excitation source. X-ray photoelectron spectra and the corresponding Auger electron spectra were recorded using a Thermo Scientific K-alpha spectrometer (Al K_α monochromatic X-ray source, Argon gun for surface etching). Optical measurements were carried out through reflectance mode using a Perkin Elmer Lambda 35 spectrophotometer.

3.2. Photoelectrochemical measurements

The PEC reduction of water $\text{H}_2\text{O} \xrightarrow{e^-/\text{hv}} \text{H}_2$ over the prepared Cu_2O

films (of surface area 0.27 cm^2 exposed through an O-ring) was carried out in a typical three-electrode cell configuration containing a saturated Ag/AgCl as the reference electrode and a large area Pt counter electrode. The potential in this manuscript has been referred with respect to reversible hydrogen electrode (RHE) using the following equation

$$E_{\text{RHE}} = E_{\text{Ag/AgCl}} + 0.197 + 0.059\text{pH} \quad (1)$$

$$(E_{\text{Ag/AgCl}} \text{ (4 M KCl)} = 0.197 \text{ V vs. NHE at } 25^\circ\text{C})$$

Linear sweep voltammetry (LSV) was carried out using the potentiostat (model CHI 650E, CH Instruments, USA) within the applied bias of 0.8 to 0.28 V vs. RHE at a scan rate of 10 mV/s in 0.1 (M) Na_2SO_4 solution in presence of 0.2 (M) sodium acetate buffer (pH 4.9). The photo-response was determined under periodic chopped illumination from Xe-arc lamp (white light source, 35 W, Hamaan, India) with an incident beam of 35 mW/cm², measured through a optical power meter (Newport, Hand-held Optical Power Meter 1916-R) coupled with a Silicon photodiode detector (Newport, Model 818-UV/DB UV). In all PEC measurements, the working electrode was front illuminated (through the electrolyte/electrode interface).

To study the hydrogen generation, the gas chromatographic (GC) method was used where the area under the Gaussian peak gives the amount of H_2 evolved. The generated H_2 in the headspace of the working electrode compartment was detected and estimated through an online GC using a YL Instrument, 6500GC system with a thermo conductive detector (TCD). In the closed container, under continuous illumination, gas bubbles were formed in 0.1 (M) Na_2SO_4 solution in presence of 0.2 (M) sodium acetate buffer (pH 4.9) with saturated argon media. The GC system was previously calibrated with hydrogen standards of high purity and was subsequently used to quantify the amount of hydrogen liberated under experimental conditions.

PEC action spectrum was obtained through chronoamperometry at constant potential 0.4 V vs. RHE under periodic monochromatic illumination using a monochromator (Oriel) and the same lamp source. Typically, the monochromator was placed in between the Xe-lamp and PEC cell in such a way that allows the monochromatic beam to illuminate the semiconductor surface through the solution and the power spectrum plot of the monochromatic beams at each of the wavelength. This potential (0.4 V vs. RHE) was selected as almost highest photocurrent was observed for all of the semiconductor and to minimize the photo-reduction of the materials that may occur at more cathodic side, similar studies were also reported in literature [5]. The incident photon to current efficiency (IPCE) was carried out on the same 3- electrode cell using same lamp with a monochromator with a bandwidth of 10 nm. IPCE was calculated according to the following equation:

$$\text{IPCE} = \frac{I_{\text{ph}} (\text{A/cm}^2)}{P_{\text{in}} (\text{W/cm}^2)} \times \frac{1240}{\lambda (\text{nm})} \times 100\% \quad (2)$$

where I_{ph} is the photocurrent (A/cm^2), P is the intensity of incident monochromatic light at a specific wavelength (W/cm^2), and λ is the incident light wavelength (nm).

Durability of the prepared pure and Cd-modified Cu_2O films undergoing PEC reduction of water in the same solution, as mentioned above, were tested through chronoamperometric i-t plot, at fixed potential 0.4 V vs. RHE for 30 min. under steady illumination of 35 mW/cm².

3.3. Electrochemical impedance spectroscopic (EIS) measurements

The EIS Nyquist plots were obtained under dark, UV-vis and visible illumination with the help of AUTOLAB 302N-FRA II. Measurements were carried out at an applied potential of 0.4 V vs. RHE (ac rms amplitude of 10 mV) within the frequency range of 100 kHz to 20 mHz using the same electrolytic solution, discussed above. Variations of capacitance of the semiconductor-electrolyte interface were derived

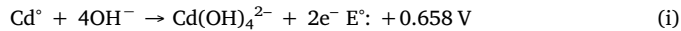
within the applied potential range of 0.3 to 0.7 V vs. RHE at three different frequencies of 1000, 500 and 200 Hz.

4. Results and discussion

Photoelectrochemical performances of p-Cu₂O semiconductors were improved through modification of the electrodeposition bath by adding different levels of Cd²⁺. During the growth of the semiconductor matrix, n-type Cd(OH)₂ buffer layer are expected to form along with the doping of Cd ion into the bulk Cu₂O to fill up the Cu deficiency and subsequently improve the p-type conductivity [24–27]. Such kind of modifications influence the overall PEC process in different ways: (i) decrease in particle size and import better crystallinity, (ii) improve electrical properties with lowering resistance, (iii) increase in carrier concentration and minimizing the charge transfer resistance, and (iv) rapid separation of photogenerated charge carrier through suppression of recombination.

Variations in E – t plot during the growth of Cu₂O film in presence and absence of Cd²⁺ during electrodeposition has been presented in Fig. S1 (Supplementary material). The figure indicates that the Cu₂O film growth process attains steady state within short period of time (within initial 600–650 sec of deposition) in absence of Cd²⁺ over Cu foil substrate. However, Cd²⁺ in the strong alkaline electrodeposition bath, exist as Cd(OH)₂ precipitate with minor amount of Cd(OH)₄²⁻, influence the film growth kinetics significantly [28]. Under reducing environment (cathodic electrodeposition), different process occur in the electrolytic bath: (i) Cd²⁺ → Cd°; (ii) Cu²⁺ → Cu¹⁺. However, over the film surface Cd undergoes spontaneous oxidation forming Cd(OH)₄²⁻ and catalyzes the Cu²⁺ → Cu¹⁺ reaction along with further reduction of Cu¹⁺ → Cu° through formation of local galvanic cells [Cd°|Cd(OH)₄²⁻||Cu²⁺|Cu¹⁺ and Cd°|Cd(OH)₄²⁻||Cu¹⁺|Cu°]. This leads to the increase in elemental Cu content in Cd-modified film, as appeared from the distinct peak at ~567.8 eV in the Auger spectral analysis of the pure and 33% Cd-modified Cu₂O samples, presented in Fig. S6 (Supplementary material).

The half-cell reactions may be represented as:



Since the reduction of Cu¹⁺ → Cu° is thermodynamically more favorable, the overall process became spontaneous, as evident from the sudden shifting of the cell potential to the cathodic side in presence of Cd²⁺ Fig. S1(Supplementary material). The potential became stable, to some extent, after 1100–1200sec of deposition due to slow down of the secondary reduction of Cu¹⁺, as the passivating Cu₂O film develops gradually. Enrichment of elemental Cu in the Cd-modified film compared to the pure Cu₂O, as detected in XRD analysis, supports the above observation.

4.1. Physicochemical characterization

Pure and Cd-modified Cu₂O films were subjected to different analyses to indentify the role of Cd over the semiconductor. Fig. 1(a i-iii) shows scanning electron microscopic (SEM) images of pure (Cu/Cu₂O), 33% and 35% Cd modified Cu₂O (Cu/Cu₂O/Cd(OH)₂) films. The surface morphology of the 25%, 30% and 45% Cd-modified samples are presented in Fig. S2 (a–c) (Supplementary material). The micrographs indicated that the film surfaces were packed with definite shaped ‘cubes’ of Cu₂O. However with addition of Cd²⁺ in the electrolytic bath, the size of the cubic particle decreases leaving with larger working surface area. It is also evident that on gradual addition Cd²⁺ (up to 33%) to the electrodeposition bath, Cd(OH)₂ buffer layer remain uniformly distributed throughout the film surface. With further increase in

the %Cd²⁺ level, the Cd(OH)₂ particles gradually agglomerated and covered the effective Cu₂O surface.

Elemental composition of the prepared films were determined via energy-dispersive X-ray spectroscopy (EDS) and Fig. 1b and Fig. S3 (Table S1, Supplementary material) of the pure Cu₂O indicates that the film surface is covered with slightly less amount of Cu than the required 2:1 stoichiometry of Cu:O, suggesting formation of ‘metal deficient’ crystallites which acts as ‘hole’ and translated to p-type conductivity, as measured through Mott-Schottky analysis, discussed later. In case of Cd-modified film, the stoichiometric difference increases with higher content of Cu. However, the excess deposited copper does not affect the ‘cationic vacant sites’, instead present as elemental Cu along with the Cu₂O matrix, as identified in XRD and XPS analysis. Increase in relative carrier concentration (obtained from Mott-Schotky analysis) for the Cd-modified samples support this observation. The composition analyses further indicate that trace amount of Cd is nearly maintained for all of the Cd-modified samples with slight increase in its content (0.2 to 0.7 at %) with rise in Cd²⁺ concentration in the electrolytic bath. Fig. 1c shows the typical cross-sectional SEM image of 33% Cd-modified Cu₂O film on Cu foil substrate measuring film thickness ~500 nm, whereas the Fig. 1d represents the corresponding elemental mapping across the film thickness, indicating uniform distribution of the major constituents (Cu, O and Cd) throughout the film matrix.

Relative change in the crystalline behavior of pure and Cd-modified Cu₂O films have been demonstrated in XRD analysis. Fig. 2a-i represents the relative XRD pattern of thin film Cu₂O on Cu foil substrates containing different levels of Cd²⁺. The plots indicate that the usual (110), (111), (200), (220), (311), and (222) peaks are prominent, confirming “cubic” crystallite structure for electrodeposited Cu₂O (standard JCPDS file no. 05-0667). Fig. 2a-ii represents the magnified XRD plots (28–36°) identifying two minor diffraction peaks at 29.4 and 35.2° corresponding to the hexagonal Cd(OH)₂ and are marked as (100) and (101) planes (JCPDS file no. 31-0228), which is clearly observed from small angle XRD analysis of 33% Cd-modified sample and are presented in Fig. S4 (Supplementary material), which were recorded at a slower scan rate (0.2°/min). No characteristics peaks of elemental Cd and CdO were observed for any of the samples, suggesting the surface remains free from their contamination, which is expected, particularly in the alkaline deposition condition. However the elemental Cd, which was supposed to form through cathodic process on electrode surface, undergo rapid galvanic reaction with Cu¹⁺ to reduce it to elemental Cu°. Different peaks at 43.3, 45.6 and 74.1° along with a very strong peak at 50.4° were identified as arising from elemental Cu (JCPDS file no. 04-0836). Increase in relative intensity of all these peaks and their broadening, particularly for the Cd-modified sample as compared to that of pure Cu₂O, as presented in Fig. 2a-iv, supports this observation. Fig. 2a-iii shows that variation of strongest (111) peak of Cu₂O indicating distinct broadening and shifting compared to that of the original peak [29] resulting from the presence of Cd(II) in the crystal matrix which can originate the microscopic and macroscopic deformation due to their difference in ionic size. Cd(II) may compensate some of the copper ionic vacant sites of the semiconductor matrix through diffusion mechanism during film growth. It is interesting to note that the relative intensities of all other peaks corresponding to ‘cubic’ Cu₂O crystallites increases with gradual addition of Cd²⁺ during the deposition process suggesting attainment of better crystallinity of Cd-modified Cu₂O.

The average size (D in nm) of the ‘cubic’ Cu₂O crystallites (using strongest (111) peak) were calculated using Scherrer equation (Eq. 3) [30]

$$D = (0.9\lambda)/\beta\cos\theta \quad (3)$$

where, λ is the X-ray wavelength (1.541 Å), β is full width at half maxima in degrees (FWHM), θ is the diffraction angle in degrees, and the variation has been presented in Fig. 2a–v (inset). Decrease in the Cu₂O crystalline size with gradual addition of Cd²⁺ in the electrolytic

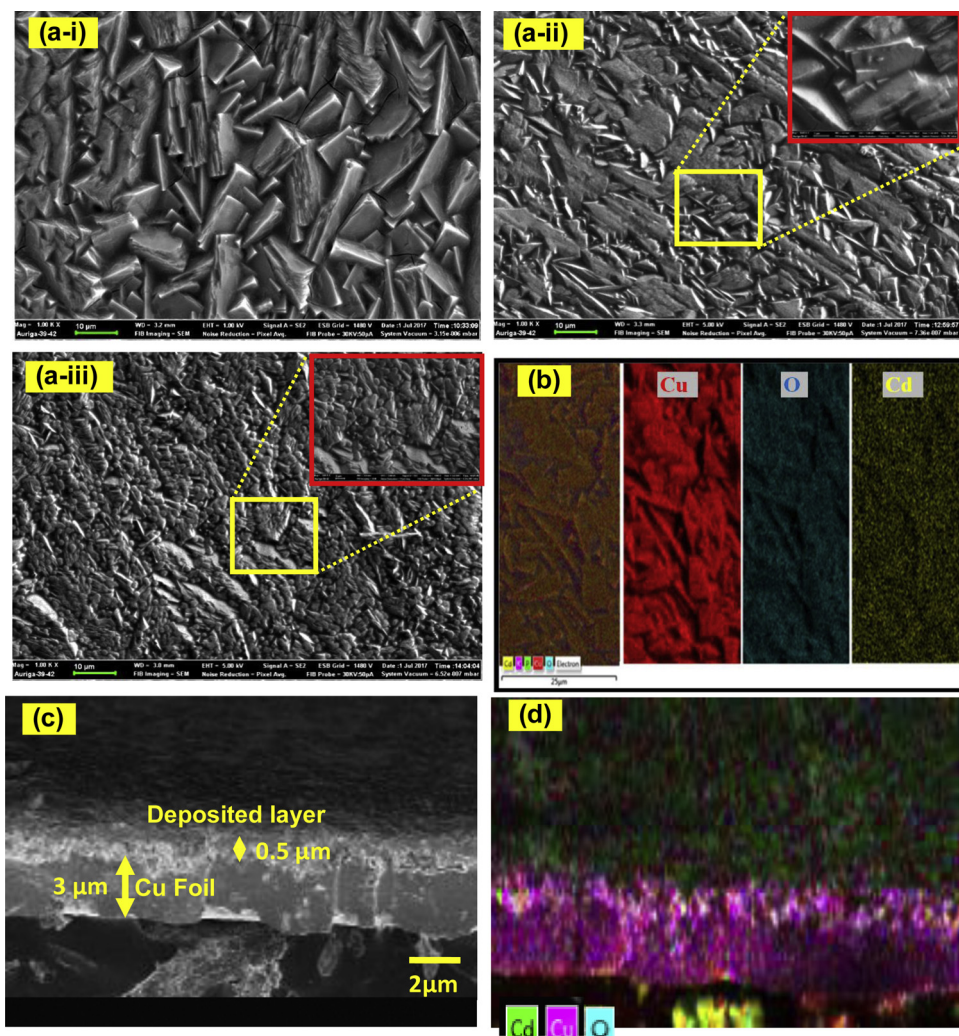


Fig. 1. (a) SEM images of (i) pure, (ii) 33% and (iii) 35% Cd-modified Cu₂O film on Cu substrate; (b) composition analysis of the optimized (33% Cd-modified) film with its (c) cross sectional image and (d) elemental mapping across the cross-section.

bath with an optimized value for the material developed with 33% Cd²⁺ indicates increase in effective surface area of the Cd-modified film and subsequently improves the overall PEC activity in the same trend, discussed later.

The influence of Cd²⁺ bath concentration on the formation of Cu₂O matrix was further studied through Raman Scattering analysis. Fig. 3a shows the Raman dispersion spectra of the different Cd-modified samples indicating unique phonon frequencies of Cu₂O crystals. The two strong peaks at 217 and 636 cm⁻¹ are attributed to the second-order Raman-allowed mode (2 Γ₁₂⁻) and the red-allowed mode of Cu₂O [31]. The sharp nature of the strongest peak demonstrates proper crystalline quality of the synthesized samples. The band at ~636 cm⁻¹ can be deconvoluted into two peaks at 632 cm⁻¹ and 650 cm⁻¹, arising due to TO-LO splitting for polar oscillations. Position of the peak at ~300 cm⁻¹ results from double-phonon scattering in Cu₂O [32,33]. The small peak at 413 cm⁻¹ has been marked to four phonon mode (3 Γ₁₂⁻ + Γ₂₅⁻) [34]. For Cd-modified samples, an increasing trend was observed in the intensities of the peaks particularly, at 147 cm⁻¹ and the two-phonon band at 217 cm⁻¹, compared to that for the one-phonon band at 636 cm⁻¹. In summary, these effects and a general trend of increasing Raman spectral intensity (Fig. 3b,c, inset), are ascribed to the restoration of electron-phonon interaction in the Cd-modified Cu₂O films indicating crystal quality improvement as supported by XRD analysis. The Raman spectral analysis of Cd(OH)₂

indicates characteristic peaks corresponding to ~238 cm⁻¹ and ~380 cm⁻¹ as reported in literature [35–37]. In our present case, appearance of very strong peak at ~218 cm⁻¹ and a moderate intense peak at ~412 cm⁻¹ arising from bulk Cu₂O matrix probably mask those two peaks from Cd(OH)₂. However, on careful analysis of the Raman spectra, particularly for the Cd-modified samples, within the range of 340–460 cm⁻¹ indicates possible presence of Cd-O vibrational mode, which is insignificant for the pure Cu₂O (Fig. 3d, inset).

XPS spectra of the pure and 33% Cd²⁺ modified Cu₂O materials have been compared in Fig. S5a (Supplementary material) indicating presence of usual C1s (at 285 eV), O1s, Cu2p_{3/2} and Cu2p_{1/2} peaks. Further, for the Cd-modified sample (Fig. S5b, inset), peaks at 405 and 411 eV corresponding to the Cd3d_{5/2} and Cd3d_{3/2}, respectively, confirms presence of traces of Cd in the film matrix. For pure Cu (I) oxide, the main peak at 932.2 eV and the secondary peak at 952.1 eV due to Cu2p_{3/2} and Cu2p_{1/2}, respectively (as presented in Fig. S5c) [38] shifted towards positive binding energies corresponding to 932.8 and 952.7 eV, in case of Cd-modified sample (Fig. S5c). Similar trend was also observed for the weak satellite at 943 eV. Appearance of two extra satellite peaks of relatively small intensities at higher binding energies of 933.6 and 962.1 eV, indicate a trace contamination of Cu(II) in the films matrix. This particular shifting binding energies of Cu2p peaks in case of Cd-modified samples implies coupling between core level electrons of Cd3d with that of Cu2p. Since, electronegativity of Cu in Cu₂O

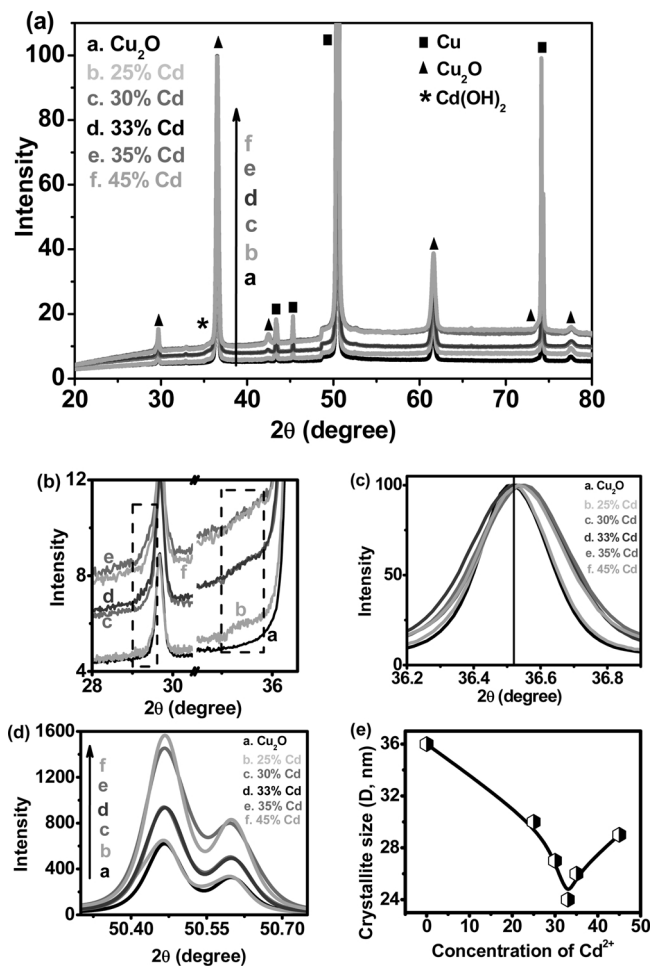


Fig. 2. (a) XRD patterns of Cu₂O films deposited from electrolytes with different level of Cd with variation of (b) Cd(OH)₂ peaks (c) Shifting and bordering of 'strongest' (111) peak (d) pure Cu (200) peak, (e) crystallite size for different semiconductors.

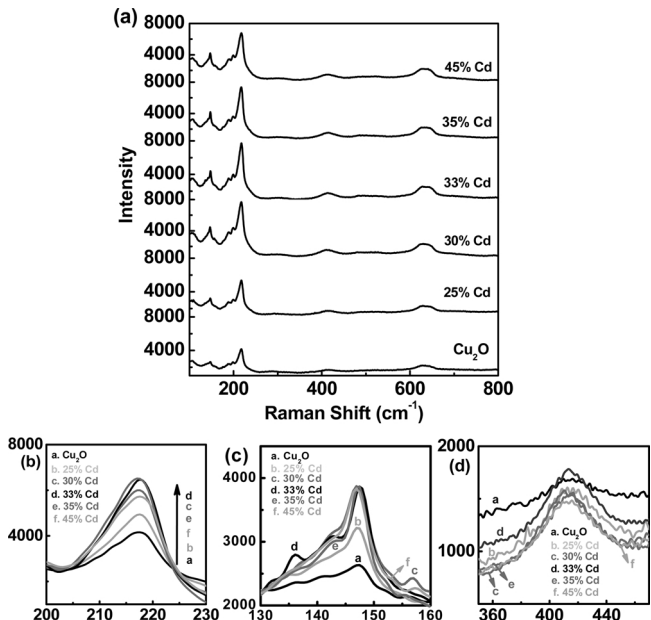


Fig. 3. (a) Raman spectra of Cu₂O films deposited from electrolytes with different level of Cd with variation of (b) strongest peak at 217 cm⁻¹, (c) 1st peak at 147 cm⁻¹ and (d) peak at 420 cm⁻¹.

is higher compared to Cd(II) hydroxide, electron-cloud density of Cu increases leaving more available electrons for H⁺ to undergo favorable reduction. Such electronic interaction at the interface of the Cu₂O and Cd(OH)₂ plays a crucial role in the overall photoelectrochemical reduction behavior of Cu/Cu₂O/Cd(OH)₂ photocathodes.

Optical characterizations of the pure and 33% Cd-modified Cu₂O films on metallic Cu-foil substrates, as obtained through reflectance measurements are presented in Fig. S7a (Supplementary material). The corresponding Tauc plot, Fig. S7b (Supplementary material), inset, indicates the respective band gap energy as 2.0 eV demonstrating almost unchanged behavior in optical properties and were used to derive the relative band positions (CB and VB) of the semiconductor electrolyte interface.

4.2. PEC analysis

Photoelectrochemical (PEC) performances of the pure and different levels of Cd-modified Cu₂O semiconductors were estimated through linear sweep voltammetry in 0.1 (M) Na₂SO₄ in presence of pH 4.9 acetate buffer solution under periodic chopped UV-vis illumination and the variation has been presented in Fig. 4a. Maximum photocurrent of -4.0 mA/cm^2 was recorded at 0.4 vs. RHE for pure Cu₂O on Cu substrate which is consistent with our earlier report [18]. However the maximum photocurrent gradually rises for the films developed in presence of increasing concentration of Cd in the electrolytic bath and reaches to its highest value (-6.1 mA/cm^2) for the material grown in presence of 33% Cd. Almost 1.5 times enhancement of photocurrent, compared to pure Cu₂O, was recorded for the optimized film (Cu/Cu₂O/33% Cd) beyond which the photocurrent again decreases for the film developed with higher Cd concentration. It is also noted that, the photocurrent onset potential (V_{on}) shifted to less cathodic side (0.72 V for pure Cu₂O to 0.85 V vs. RHE) for the Cd-modified samples indicating better catalytic behavior of these materials. Idealized I-V plots of the modified samples also support this observation [39–41]. Increasing trend of photocurrent for the samples prepared in the initial concentration ranges of Cd is primarily due to lowering of the resistance of the photocathode through moderate diffusion of Cd from the overlayer in to the bulk Cu₂O matrix resulting in increase of hole concentration. The Cd-modification further improves crystallinity thereby facilitates carrier mobilities resulting in rapid electron transfer to the electrolyte through the formation of conduction band discontinuation in presence of Cd(OH)₂ buffer layer thus suppress the recombination at the Cu₂O surface.

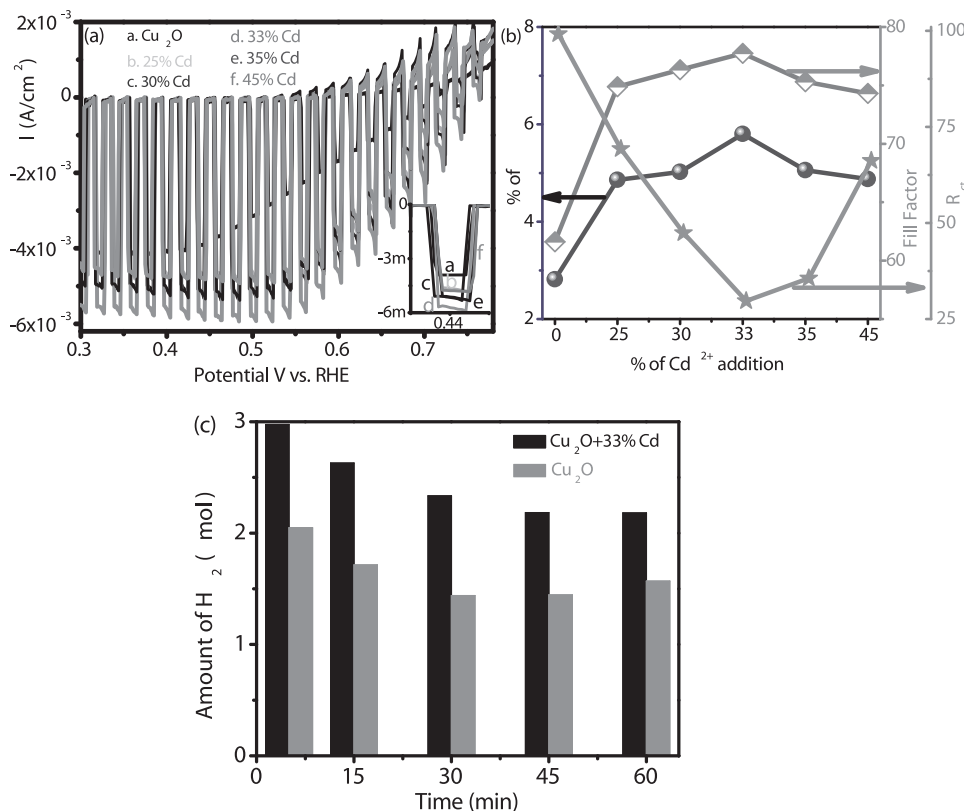
However lowering of photocurrent at higher concentrations of Cd²⁺ ($\geq 35\%$) may be explained due to the over diffusion of Cd ion into Cu vacant site of p-type Cu₂O film with lowering of carrier concentrations, and accumulation of excess Cd(OH)₂ may reduce the life time of photogenerated charge carrier, via recombination through defect sites near the interface before it reaches the depletion layer.

When the photocathodes were illuminated with high power Xe arc lamp (100 mW/cm^2 illumination) the photocurrent increases to -6.9 mA/cm^2 for 33% Cd modified Cu₂O, whereas that for pure sample as -4.6 mA/cm^2 which is presented in Fig. S8 (Supplementary material).

Fig. 4b shows the variations of % η (optical to electrical energy conversion efficiency) and %FF (fill factor) of the different semiconductors as derived from the respective I-V plots. Maximum photoconversion efficiency of 2.8% was calculate for pure Cu₂O which improves almost two fold to 5.8% for 33% Cd-modified sample using following equation. The fill factor also found to enhance, from 61 to 77%, suggesting better charge-transfer kinetics over the Cd-modified Cu₂O/Cd(OH)₂ system.

$$\% \eta = (I_{max} \times V_{max}) / P_{input} \quad (4)$$

Fig. 4c shows the photocatalytic H₂ generation through water reduction using pure and 33% Cd-modified Cu₂O semiconductors thin



films (1 cm x 1 cm) in 0.1 M Na₂SO₄ in presence of pH 4.9, acetate buffer solution at 0 V under visible light irradiation ($\lambda > 390$ nm). 33% Cd modified Cu₂O photocathodes exhibits 1.5 times photocatalytic H₂ generation (2.9 μmol) compare to pure Cu₂O (2.0 μmol). The faradaic efficiency (%FE) was calculated from the amount of H₂ generated and the chronoamperometric i-t plot. Pure Cu₂O exhibits 36% efficiency whereas the 33% Cd-modified sample shows 45% efficiency.

Fig. 5a shows the dispersion of incident photon to current conversion efficiencies (IPCE) as derived from the respective PEC action spectrum (I_{ph} - λ plot), presented in Fig. S10a,b (supplementary material) using pure and Cd-modified Cu/Cu₂O photocathodes measured at 0.4 V vs. RHE under monochromatic front side illumination. Variation of maximum IPCE, measured for each of the sample has been presented in Fig. 5b, inset. 44% IPCE was recorded for the pure Cu₂O which increases to almost two-fold in presence of 33% Cd-modified sample. The figure (Fig. 5b) also represents the PEC band gap of the individual semiconductor as calculated from the Tauc plot (Fig. S11, Supplementary material) from IPCE spectra indicating slight decrease in the band gap energy with Cd-modification, favoring photoelectrochemical behavior of the semiconductors.

The photo-stability of the different photocathodes was tested through chronoamperometric i-t curve at a constant applied potential of 0.4 V vs. RHE under steady illumination and successive LSV scans under periodic illumination using the same electrolytic solution. Fig. 5c represents the i – t plots of the electrodes developed in presence of different % of Cd²⁺, whereas Fig. S13 (a,b) represents the repeated LSV scan for 33% Cd-modified and pure Cu₂O. Although the photo-degradation of Cu₂O was well known [42,43], particularly in aqueous environment, slight improvement in its stability was achieved for the semiconductors developed in presence of moderate concentrations of Cd²⁺ in the electrodeposition bath, as presented in Fig. 5d, inset, which is also supported from Fig. S13 (a,b). The optimized Cd-modified Cu₂O was found to retain ~68, 58 and 55% of its initial photocurrent (at 200 s) after 600, 1200 and 1600 sec of illumination, respectively. Whereas the pure Cu₂O suffers significant loss in photoactivity at same

Fig. 4. (a) LSV plots and variations of (b) solar energy conversion efficiencies (% η), fill factor (%FF) and charge transfer resistance (R_{ct}); (c) GC analysis for H₂ generation under 100 mW cm⁻² (visible light) for different Cu₂O films undergoing photoelectrochemical reduction of water (in presence of 0.1 M Na₂SO₄ electrolyte: pH 4.9).

time ~61, 47 and 31%, respectively, indicating better applicability of the Cd-modified sample over pure Cu₂O semiconductor. The effect may be explained by the fact that the photo-generated electrons, which was responsible for self-reduction (degradation) of the Cu₂O semiconductor, transferred spontaneously to the electrolyte (H⁺) to produce H₂ via Cd(OH)₂ through conduction band alignment, thereby preventing from photo-corrosion. SEM images and XRD analysis of pure and 33% Cd modified Cu₂O films after chronoamperometric measurement, reveals the presence of Cu nano particles at the surface of the materials and represented in Fig. S14 (Supplementary material).

4.3. Impedance measurements

Modifications of Cu₂O by incorporation of Cd ion and Cd(OH)₂ buffer layer were further analyzed through electrochemical impedance spectroscopy (EIS) in the electrolytic solution under dark and illuminated condition. The complex impedance spectra (Nyquist plot) were obtained for the different semiconductors at 0.4 V vs. RHE and are presented in Fig. 6a. Analysis of the spectra reveals the detailed photo-generated carrier activity in the bulk semiconductor matrix and charge transfer kinetics across the semiconductor-electrolyte interface. Single semicircular nature of the Nyquist plots confirms simple charge transfer process across the interface and was fitted with the Randles equivalent circuit (EC) model [44], Fig. 6c, (inset). The high-frequency limit of the Nyquist plot indicates the ohmic resistances (R_s), whereas the diameter of the semicircle is correlated to the charge transfer resistance (R_{ct}) associated with the double layer, having capacitance C_{dl}. High frequency region of the Nyquist plots, as presented in the magnified portion, Fig. 6b, inset reveals lowering of the ohmic resistance (R_s) value with gradual addition of Cd²⁺ to the electrolytic bath compared to the pure Cu₂O. Modification of the semiconductor crystallites with incorporation of Cd²⁺ and presence of elemental Cu, as identified in XRD analyses, supports this observation. Increasing trend in R_s for the films developed with higher Cd²⁺ concentrations is attributed to the accumulation of excess Cd(OH)₂ which acts as barrier for the

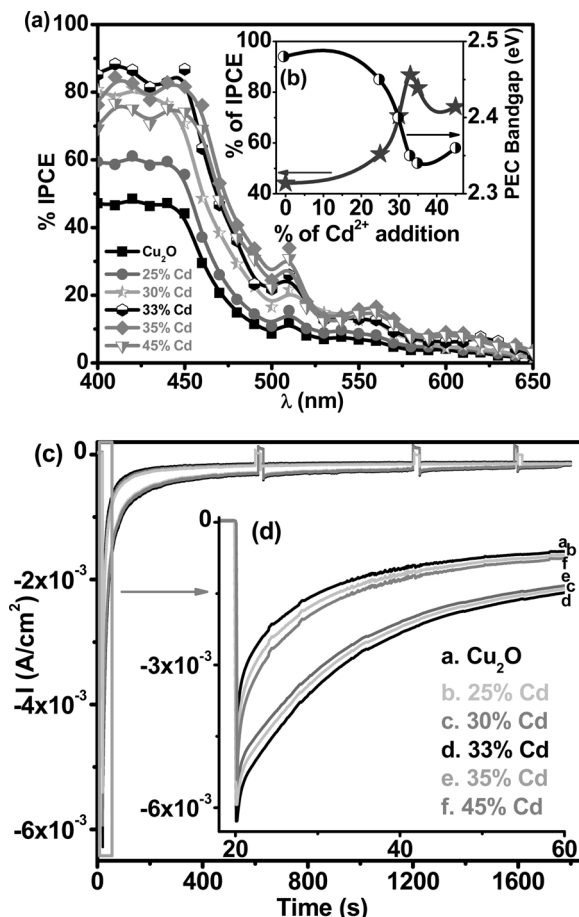


Fig. 5. (a) IPCE spectra; (b, inset) highest %IPCE and band gap energy; (c) chronoamperometric stability plot and (d) magnified portion of the stability plot for different Cu_2O films undergoing photoelectrochemical reduction of water (in presence of 0.1 M Na_2SO_4 electrolyte: pH 4.9).

semiconductors. It is also evident that the R_{ct} decreases significantly in presence of Cd^{2+} and attains the minima at 33% Cd-modified film indicating a most favourable condition for charge transfer process at the interface, similar to the observation discussed in photoelectrochemical performance studies (presented in Fig. 4b). Fig. 6d represents the Bode phase plot of the corresponding impedance data shown in Fig. 6a. It was evident that with increase in % Cd in the electrolytic bath, the maximum phase shift shifted towards higher frequency region indicating favorable charge transfer process across the semiconductor-electrolyte interface compared to diffusion within the electrolyte [45]. The corresponding transit time (τ_t) calculated from the characteristic frequency at the peak of high-frequency region using following equation and are presented in Table 1, indicating addition of an optimized amount of Cd^{2+} leads to significant decrease in transit time.

$$\tau_t = 1/2\pi f \quad (5)$$

Therefore, under illumination, photo-generated charge carriers rapidly transported in the depletion layer of $\text{Cu}_2\text{O}/\text{Cd}(\text{OH})_2$ than pure Cu_2O , which is consistent with the results obtained from the Mott-Schottky analysis, discussed later. With gradual increase in % Cd it was observed that the maximum phase shift decreases and reaches to its lowest value for 33% Cd-modified film, suggesting better resistive behavior for that material which intern facilitates the charge transfer kinetics.

Fig. S15 (Supplementary material) represents the typical Nyquist plots for the optimized sample ($\text{Cu}/\text{Cu}_2\text{O}/33\%\text{Cd}$) under dark, visible and UV-vis illumination. Order of the R_{ct} as estimated from the

diameter of the respective semicircle (Table S2, Supplementary material) follows the trend as: dark > > visible > UV-vis. Significant decrease in R_{ct} value under UV-vis illumination as compared to visible light, suggest the buffer mechanism of $\text{Cd}(\text{OH})_2$ layer, which is purely UV-active, by faster transfer of photo-generated electrons to the electrolyte thus enhancing PEC activity of the modified semiconductors.

Variations of carrier concentration through Cd modifications were investigated through Mott-Schottky analysis. A typical 1 kHz frequency was applied to carry out the experiment within the potential range 0.3–0.7 V vs. RHE using the same electrolyte as stated earlier. The variation in space charge capacitance ($1/C_{sc}^2$) at different applied bias (E) has been presented in Fig. 6e, and analyzed using the Mott-Schottky equation [46]:

$$1/C_{sc}^2 = (2/e\epsilon\epsilon_0 N_A)(E - E_{fb} - kT/e) \quad (6)$$

where C_{sc} is the space-charge capacitance, in F cm⁻², ϵ is the dielectric constant of the semiconductors [47,48]; e is the electronic charge in C; N_A is the carrier (hole) density in cm⁻³; ϵ_0 is the permittivity of free space; E_{fb} is the flat band potential in V; k is the Boltzmann constant; and T is the temperature in K. Negative slope of the plots indicates p-type conductivity of the materials. The frequency independent behaviour of the semiconductors were verified at three different frequencies of 1000, 500 and 200 Hz using the optimized sample, as shown in Fig. S16a (Supplementary material). The Mott-Schottky plot for the bare $\text{Cd}(\text{OH})_2$ film developed under similar experimental condition has been presented in Fig. S16b (Supplementary material) for comparison, showing different characteristics to the Cd modified samples. The flat-band potential (E_{fb}) estimated from the intercept at potential axis as 0.61 V vs. RHE and N_A from the slope are presented in Table 1. Almost five-fold increase in the hole concentration for the optimized sample over pure semiconductor may be attributed to the fact that Cd modifies the Cu_2O crystallites through diffusion of Cd^{2+} into the matrix and generates metal deficiency. The charge carrier diffusion length (Debye length, L_D) for all photocathodes as presented in Table 1, were calculated using following equation [49,50];

$$L_D = \sqrt{\frac{\epsilon\epsilon_0 kT}{e^2 N_A}} \quad (7)$$

Addition of Cd^{2+} to the electrodeposition bath leads to the modified semiconductor with significant decrease in the L_D value and in particular for the optimized sample (33% Cd) the value reaches to the $\frac{1}{2}$ of that for the pure Cu_2O . Since the transit time through depletion region is proportional to the square of the diffusion length L_D , 33% Cd-modified Cu_2O exhibits fast transport properties. The depletion layer width (W), was calculated according to following equation [51] and are reported in Table 1

$$W = \sqrt{\frac{2\epsilon\epsilon_0 |\Phi|}{e^2 N_A}} \quad (8)$$

where $|\Phi| = E - E_{fb}$, is the maximum potential drop in the depletion region. The optimized semiconductor having much smaller depletion layer width than pure Cu_2O , results in the reduction of charge transport resistance and thus favors PEC performances.

Fig. 6f shows the relative band position of conduction band (CB) and valence band (VB) of $\text{Cu}/\text{Cu}_2\text{O}/33\%\text{Cd}(\text{OH})_2$, using the values of optical band gap energy and flat band potential. Presence of $\text{Cd}(\text{OH})_2$ shifts the CB positions favorable for reduction of water ($\text{H}_2\text{O} \rightarrow \text{H}_2$) in comparison to that for pure Cu_2O , thereby favoring PEC generation of H_2 through reduction of water, as evident from LSV and IPCE measurements.

5. Conclusion

We have demonstrated a successful one pot electro-synthetic procedure to develop a Cd-modified Cu_2O photocathode with high

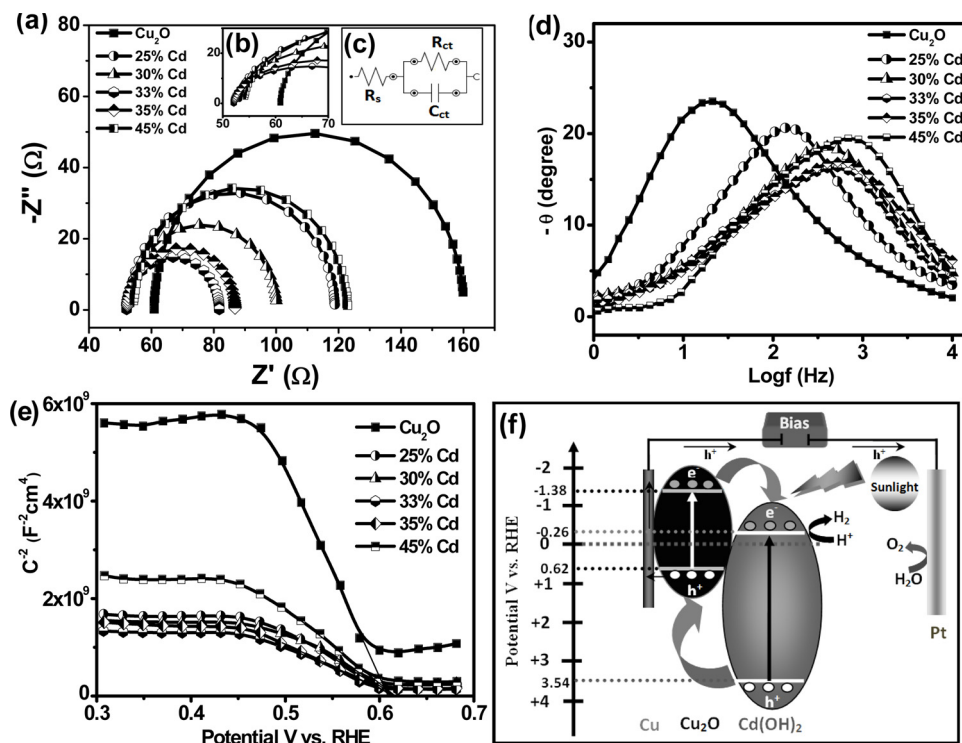


Fig. 6. (a) Nyquist plots (at 0.4 V vs. RHE); (b, inset) magnified portion in the high frequency region; (c) Equivalent circuit model; (d) Bode phase plots (e) Mott-Schottky plots of the different Cu₂O films in 0.1 M Na₂SO₄ electrolytes (pH 4.9) and (f) Schematic band diagram for PEC reduction of water.

Table 1
Fundamental electronic parameters from electrochemical impedance analyses.

Sample	Carrier Density (10^{19} cm^{-3})	Debye Length (Å)	Width of depletion layer (nm, 0 V vs RHE)	Transit time τ_t (ms)
Cu/Cu ₂ O	6.46	3.7	2.65	7.5
Cu/Cu ₂ O/25%Cd	28.7	1.8	1.23	1.2
Cu/Cu ₂ O/30%Cd	28.7	1.8	1.22	0.4
Cu/Cu ₂ O/33%Cd	32.3	1.7	1.15	0.3
Cu/Cu ₂ O/35%Cd	32.3	1.7	1.16	0.3
Cu/Cu ₂ O/45%Cd	25.8	1.9	1.3	0.2

efficiency towards water splitting reaction. The synergistic effect of Cd²⁺ through the formation of p-type dopant and forming a Cd(OH)₂ buffer layer over the Cu₂O surface with (i) importing better crystallinity, (ii) increasing carrier concentration, (iii) minimizing the interfacial resistance and (iv) rapid separation charge carriers preventing the recombination process. The optimized level of Cd²⁺ (33%) modified Cu₂O generates maximum water reduction photocurrent -6.1 mA/cm², a 1.5 times higher than that of pure Cu₂O. The solar energy conversion efficiency also significantly increases up to 5.8%.

Acknowledgements

This work was financially supported by Board of Research in Nuclear Science (BRNS), Department of Atomic Energy, Government of India, sponsored project (Ref. No. 2013/37C/61/BRNS) and Financial assistance from SERB-DST, Govt. of India (File no. SB/S1/PC-042/2013), and DST, Govt. of West Bengal, (File no. 902(Sanc.)/ST/P/S & T/4 G – 1/2013) to the Department of Chemistry, IEST, Shibpur are gratefully acknowledged.

Appendix A. Supplementary data

Supplementary material related to this article can be found, in the online version, at doi:<https://doi.org/10.1016/j.apcatb.2019.01.017>.

References

- [1] T. Wang, Z. Luo, C. Li, J. Gong, Controllable fabrication of nanostructured materials for photoelectrochemical water splitting via atomic layer deposition, *Chem. Soc. Rev.* 43 (2014) 7469–7484, <https://doi.org/10.1039/C3CS60370A>.
- [2] F.E. Osterloh, Inorganic nanostructures for photoelectrochemical and photocatalytic water splitting, *Chem. Soc. Rev.* 42 (2013) 2294–2320, <https://doi.org/10.1039/C2CS35266D>.
- [3] A. Paracchino, J. Brauer, J.E. Moser, E. Thimsen, M. Graetzel, Synthesis and Characterization of high-photoactivity electrodeposited Cu₂O solar absorber by photoelectrochemistry and ultrafast spectroscopy, *J. Phys. Chem. C.* 116 (2012) 7341–7350, <https://doi.org/10.1021/jp301176y>.
- [4] J.N. Nian, C.C. Hu, H. Teng, Electrodeposited p-type Cu₂O for H₂ evolution from photoelectrolysis of water under visible light illumination, *Int. J. Hydrogen Energy* 33 (2008) 2897–2903, <https://doi.org/10.1016/j.ijhydene.2008.03.052>.
- [5] T. Minami, Y. Nishi, T. Miyata, J. Nomoto, High-efficiency oxide solar cells with ZnO/Cu₂O heterojunction fabricated on thermally oxidized Cu₂O sheets, *Appl. Phys. Expr.* 4 (2011) 062301–062303, <https://doi.org/10.1143/APEX.4.062301>.
- [6] D. Sharma, S. Upadhyay, V.R. Satsangi, R. Srivastav, U.V. Waghmare, S. Dass, Improved photoelectrochemical water splitting performance of Cu₂O/SrTiO₃ heterojunction photoelectrode, *J. Phys. Chem. C.* 118 (2014) 25320–25329, <https://doi.org/10.1021/jp507039n>.
- [7] T. Minami, Y. Nishi, T. Miyata, Impact of incorporating sodium into polycrystalline p-type Cu₂O for heterojunction solar cell applications, *Appl. Phys. Lett.* 105 (2014) 212104, <https://doi.org/10.1063/1.4902879>.
- [8] C. Bhattacharya, H.C. Lee, A.J. Bard, Rapid screening by scanning electrochemical microscopy (SECM) of dopants for Bi₂WO₆ improved photocatalytic water oxidation with Zn doping, *J. Phys. Chem. C.* 117 (2013) 9633–9640, <https://doi.org/10.1021/jp308629q>.
- [9] B. O'Regan, M. Gratzel, A low-cost, high-efficiency solar cell based on dye-sensitized colloidal TiO₂ films, *Nature* 335 (1991) 737–740, <https://doi.org/10.1038/353737a0>.

- [10] S.D. Tilley, M. Schreier, J. Azevedo, M. Stefk, M. Graetzel, Ruthenium oxide hydrogen evolution catalysis on composite cuprous oxide water-splitting photocathodes, *Adv. Funct. Mater.* 24 (2014) 303–311, <https://doi.org/10.1002/adfm.201301106>.
- [11] D. Wu, Y. Wei, X. Ren, X. Ji, Y. Liu, X. Guo, Z. Liu, A.M. Asiri, Q. Wei, X. Sun, Co(OH)₂ nanoparticle-encapsulating conductive nanowires array: room-temperature electrochemical preparation for high-performance water oxidation electrocatalysis, *Adv. Mater.* 30 (2018) 1705366–1705372, <https://doi.org/10.1002/adma.201705366>.
- [12] X. Ren, R. Ge, Y. Zhang, D. Liu, D. Wu, X. Sun, B. Du, Q. Wei, Cobalt–borate nanowire array as a high-performance catalyst for oxygen evolution reaction in near-neutral media, *J. Mater. Chem. A Mater. Energy Sustain.* 5 (2017) 7291–7294, <https://doi.org/10.1039/c7ta01027c>.
- [13] X. Ren, D. Wu, R. Ge, X. Sun, H. Ma, T. Yan, Y. Zhang, B. Du, Q. Wei, L. Chen, Self-supported CoMoS₄ nanosheet array as an efficient catalyst for hydrogen evolution reaction at neutral pH, *Nano Res.* 11 (2018) 2024–2033, <https://doi.org/10.1007/s12227>.
- [14] X. Ren, X. Ji, Y. Wei, D. Wu, Y. Zhang, M. Ma, Z. Liu, A.M. Asiri, Q. Wei, X. Sun, In situ electrochemical development of copper oxide nanocatalysts within a TCNO nanowire array: a highly conductive electrocatalyst for the oxygen evolution reaction, *Chem. Commun.* 54 (2018) 1425–1428, <https://doi.org/10.1039/C7CC08748A>.
- [15] Y. Wei, X. Ren, H. Ma, X. Sun, Y. Zhang, X. Kuang, T. Yan, H. Ju, D. Wu, Qin Wei, CoC₂O₄·2H₂O derived Co₃O₄ nanorods array: a high-efficiency 1D electrocatalyst for alkaline oxygen evolution reaction, *Chem. Commun.* 54 (2018) 1533–1536, <https://doi.org/10.1039/C7CC08423D>.
- [16] J. Zhao, X. Ren, Q. Han, D. Fan, X. Sun, X. Kuang, Q. Wei, D. Wu, Ultra-thin wrinkled NiOOH–NiCr₂O₄nanosheets on Ni foam: an advanced catalytic electrode for oxygen evolution reaction, *Chem. Commun.* 54 (2018) 4987–4990, <https://doi.org/10.1039/C8CC01002A>.
- [17] S. Chen, S. Perathoner, C. Ampelli, C. Mebrahtu, D. Su, G. Centi, Room-temperature electrocatalytic synthesis of NH₃ from H₂O and N₂ in a gas–liquid–solid three-phase reactor, *ACS Sustain. Chem. Eng.* 5 (2017) 10093–10098, <https://doi.org/10.1021/acssuschemeng.7b01742>.
- [18] S. Shyamal, P. Hajra, H. Mandal, J.K. Singh, A.K. Satpati, S. Pande, C. Bhattacharya, Effect of substrates on the photoelectrochemical reduction of water over cathodically electrodeposited pType Cu₂O thin films, *ACS Appl. Mater. Interfaces* 7 (2015) 18344–18352, <https://doi.org/10.1021/acsami.5b04116>.
- [19] S. Shyamal, P. Hajra, H. Mandal, A. Bera, D. Sariket, A.K. Satpati, S. Kundu, C. Bhattacharya, Benign role of Bi on an electrodeposited Cu₂O semiconductor towards photo-assisted H₂ generation from water, *J. Mater. Chem. A Mater. Energy Sustain.* 4 (2016) 9244–9252, <https://doi.org/10.1039/C6TA03237K>.
- [20] D. Trivich, E.Y. Wang, R.J. Komp, A.S. Kakar, Washington, DC IEEE, *New York Proceedings of the 13th IEEE Photovoltaic Specialists Conference 1978, Proceedings of the 13th IEEE Photovoltaic Specialists Conference (1978)* 174–179.
- [21] L.C. Olsen, F.W. Addis, W. Miller, Experimental and theoretical studies of Cu₂O solar cells, *Sol. Energy Mater. Sol. Cells* 7 (1982) 247–279, [https://doi.org/10.1016/0379-6787\(82\)90050-3](https://doi.org/10.1016/0379-6787(82)90050-3).
- [22] Y.S. Lee, D. Chua, R.E. Brandt, S.C. Siah, J.V. Li, J.P. Mailoa, S.W. Lee, R.G. Gordon, T. Buonassisi, Atomic layer deposited gallium oxide buffer layer enables 1.2 V open-circuit voltage in cuprous oxide solar cells, *Adv. Mater.* 26 (2014) 4704–4710, <https://doi.org/10.1002/adma.201401054>.
- [23] A. Paracchino, V. Laporte, K. Sivila, M. Grätzel, E. Thimsen, Highly active oxide photocathode for photoelectrochemical water reduction, *Nat. Mater.* 10 (2011) 456–461, <https://doi.org/10.1038/nmat3017>.
- [24] L. Papadimitriou, Acceptor states distributed in energy in Cd-doped Cu₂O, *Solid State Comm.* 71 (1989) 181–185, [https://doi.org/10.1016/0038-1098\(89\)90398-0](https://doi.org/10.1016/0038-1098(89)90398-0).
- [25] L. Papadimitriou, C.A. Dimitriadis, L. Dozsa, L. Andor, Deep trap levels in cuprous oxide, *Solid. Electron.* 32 (1989) 445–448, [https://doi.org/10.1016/0038-1101\(89\)90026-9](https://doi.org/10.1016/0038-1101(89)90026-9).
- [26] M.M. Fadlallah, U. Eckern, U. Schwingenschlögl, Defect engineering of the electronic transport through cuprous oxide interlayers, *Sci. Rep.* 6 (2016) 27049, <https://doi.org/10.1038/srep27049>.
- [27] M. Tapiero, C. Noguet, J.P. Zielinger, C. Schwab, D. Pierrat, Photovoltaic conversion in Cu₂O, *Aggressologie* 14 (1979) 231–236, <https://doi.org/10.1051/rphysap:01979001401023100>.
- [28] A.I. Demidov, Thermodynamics of reactions involving zinc and cadmium ions in alkaline solutions, *Russian J. Appl.Chem.* 80 (2007) 1181–1182, <https://doi.org/10.1134/S1070427207070336>.
- [29] H. Kato, K. Asakura, A. Kudo, Highly efficient water splitting into H₂ and O₂ over lanthanum-doped NaTaO₃ photocatalysts with high crystallinity and surface nanostructure, *J. Am. Chem. Soc.* 125 (2003) 3082–3089, <https://doi.org/10.1021/ja027751g>.
- [30] P. Scherrer, Bestimmung der GröÙe und der inneren Struktur von Kolloidteilchen mittels RöÙtgenstrahlen, *Nachr. Ges. Wiss. Göttingen* 26 (1918) 98–100.
- [31] D. Powell, A. Compaan, J.R. Macdonald, R.A. Forman, Raman-scattering study of ion-implantation-produced damage in Cu₂O, *Phys. Rev. B* 12 (1975) 20–25, <https://doi.org/10.1103/PhysRevB.12.20>.
- [32] P.F. Williams, S.P.S. Porto, Symmetry-forbidden resonant raman scattering in Cu₂O, *Phys. Rev. B* 8 (1973) 1782–1785, <https://doi.org/10.1103/PhysRevB.8.1782>.
- [33] H. Hagemann, H. Bill, W. Sadowski, E.M. Walker, M. Francois, Raman spectra of single crystal CuO, *Solid State Comm.* 73 (1990) 447–451, [https://doi.org/10.1016/0038-1098\(90\)90048-G](https://doi.org/10.1016/0038-1098(90)90048-G).
- [34] P.Y. Yu, Y.R. Shen, Resonance Raman studies in Cu₂O. I. The phonon-assisted 1syellow excitonic absorption edge, *Phys. Rev. B* 12 (1975) 1377–1394, <https://doi.org/10.1103/PhysRevB.12.1377>.
- [35] S.H. Shim, S. Rekhi, M.C. Martin, R. Jeanloz, Vibrational spectroscopy and x-ray diffraction of Cd(OH)₂ to 28 GPa at 300 K, *Phys. Rev. B* 74 (2006) 024107, <https://doi.org/10.1103/PhysRevB.74.024107>.
- [36] P. Rawat, R. Nagarajan, Cd(OH)F: synthesis, structure, optical and photocatalytic properties, *J. Fluor. Chem.* 182 (2016) 98–103, <https://doi.org/10.1016/j.jfluchem.2015.12.006>.
- [37] H.D. Lutz, H. Mdller, M. Schmidt, Lattice vibration spectra. Part LXXXII. Brucite-type hydroxides M(OH)₂ (M = Ca, Mn, Co, Fe, Cd) — IR and Raman spectra, neutron diffraction of Fe(OH)₂, *J. Molecular Structure* 328 (1994) 121–132, [https://doi.org/10.1016/0022-2860\(94\)80355-X](https://doi.org/10.1016/0022-2860(94)80355-X).
- [38] C.K. Mavrokefalos, M. Hasan, J.F. Rohan, R.G. Compton, J.S. Foord, Electrochemically deposited Cu₂O cubic particles on boron doped diamond substrate as efficient photocathode for solar hydrogen generation, *Appl. Surf. Sci.* 408 (2017) 125–134, <https://doi.org/10.1016/j.apsusc.2017.02.148>.
- [39] H. Ye, J. Lee, J.S. Jang, A.J. Bard, Rapid screening of BiVO₄-based photocatalysts by scanning electrochemical microscopy (SECM) and studies of their photoelectrochemical properties, *J. Phys. Chem. C* 114 (2010) 13322–13328, <https://doi.org/10.1021/jp104343b>.
- [40] K.C. Leonard, K.M. Nam, H.C. Lee, S.H. Kang, H.S. Park, A.J. Bard, ZnWO₄/WO₃ composite for improving photoelectrochemical water oxidation, *J. Phys. Chem. C* 117 (2013) 15901–15910, <https://doi.org/10.1021/jp403506a>.
- [41] H.C. Lee, S.K. Cho, H.S. Park, K.M. Nam, A.J. Bard, Visible light photoelectrochemical properties of PbCrO₄, Pb₂CrO₅, and Pb₃CrO₈, *J. Phys. Chem. C* 121 (2017) 17561–17568, <https://doi.org/10.1021/acs.jpcc.7b03230>.
- [42] Z. Zhangab, P. Wang, Highly stable copper oxide composite as an effective photocathode for water splitting via a facile electrochemical synthesis strategy, *J. Mater. Chem.* 22 (2012) 2456–2464, <https://doi.org/10.1039/C1JM14478B>.
- [43] C. Li, Y. Li, J.-J. Delaunay, A novel method to synthesize highly photoactive Cu₂O microcrystalline films for use in photoelectrochemical cells, *ACS Appl. Mater. Interfaces* 6 (2014) 480–486, <https://doi.org/10.1021/acs.nanolett.5b04929>.
- [44] B. Klahr, S. Gimenez, S.F. Fabregat, T. Hamann, J. Bisquert, Water oxidation at hematite photoelectrodes: the role of surface states, *J. Am. Chem. Soc.* 134 (2012) 4294–4302, <https://doi.org/10.1021/ja210755h>.
- [45] T. Lopes, L. Andrade, H.A. Ribeiro, A. Mendes, Characterization of photoelectrochemical cells for water splitting by electrochemical impedance spectroscopy, *Int. J. Hydrogen Energy* 35 (2010) 11601–11608, <https://doi.org/10.1016/j.ijhydene.2010.04.001>.
- [46] A.J. Bard, L.R. Faulkner, *Electrochemical Methods Fundamentals and Application*, 2nd ed., John Wiley & Sons, New York, 2001.
- [47] E.C. Heltemes, Far-infrared properties of cuprous oxide, *Phys. Rev.* 141 (1966) 803–805, <https://doi.org/10.1103/PhysRev.141.803>.
- [48] F. Pei, S. Wu, G. Wang, M. Xu, Y.S. Wang, L. Chen, Electronic and optical properties of noble metal oxides M₂O (M = Cu, Ag and Au): first-principles study, *J. Korean Phys. Soc.* 55 (2009) 1243–1249, <https://doi.org/10.3938/jkps.55.1243>.
- [49] C. Fàbrega, S.D. Monllor, S. Ampudia, A. Parra, T. Andreu, J.R. Morante, Tuning the fermi level and the kinetics of surface states of TiO₂ nanorods by means of ammonia treatments, *J. Phys. Chem. C* 117 (2013) 20517–20524, <https://doi.org/10.1021/jp407167z>.
- [50] W. Yuan, J. Yuan, J. Xie, C.M. Li, Polymer-mediated self-assembly of TiO₂@Cu₂O core – shell nanowire array for highly efficient photoelectrochemical water oxidation, *ACS Appl. Mater. Interfaces* 8 (2016) 6082–6092, <https://doi.org/10.1021/acsami.6b00030>.
- [51] X. Wang, J. Xie, C.M. Li, Architecting smart “umbrella” Bi₂S₃/rGO-modified TiO₂ nanorod array structures at the nanoscale for efficient photoelectrocatalysis under visible light, *J. Mater. Chem. A Mater. Energy Sustain.* 3 (2015) 1235–1242, <https://doi.org/10.1039/C4TA05846A>.